Geoscience Letters

RESEARCH LETTER

Open Access

Spatiotemporal slip distribution associated with the 2012–2016 Tokai long-term slow slip event inverted from GNSS data

Yukinari Seshimo[1], Hiroki Kawabata[1*], Shoichi Yoshioka[1,2] and Francisco Ortega-Culaciati[3,4]

Abstract

We used Global Navigation Satellite System (GNSS) time series data to estimate the spatiotemporal slip distribution for a long-term slow slip event (L-SSE) that occurred in the Tokai region, central Japan, from 2012 to 2016. Since all the used GNSS data were affected by the postseismic deformation associated with the 2011 Mw9.0 Tohoku-Oki earthquake, we removed such postseismic signal from the time series of three components at each of the stations. The minimal time window for an inversion analysis was set to 0.5 years (6 months), taking into account the signal-to-noise ratio of displacements for each time window. In the horizontal displacement fields, displacements were observed in the south—southeast and southeast directions on the west and east sides of Lake Hamana, respectively, with temporal changes in their amounts and directions. In the vertical displacement fields, uplift was observed on the east side of Lake Hamana. From these data, we estimated the L-SSE initiated in approximately 2012.5 and ended by 2017.0, indicating the duration time is 4.5 years and the duration was much longer than that obtained in a previous study. Using these data, we performed the inversion analysis, in which three a priori information were assumed, i.e., the spatial distribution of slip is smooth, slip mainly occurs in the direction of plate convergence, and the temporal variation in the slip is smooth, to obtain the spatiotemporal slip distribution on a plate boundary with 3-D geometry. As a result, we identified that the L-SSE consisted of two subevents. The first subevent initiated on the southwest side of Lake Hamana and expanded during the period from 2013.0 to 2014.5. The maximum slip velocity during the period from 2012.5 to 2017.0 was estimated to be approximately 3.5 cm/year there for 2013.5–2014.0. The second subevent took place on the west side of Lake Hamana gradually from 2015.0 to 2015.5, continued, and expanded from 2015.5 to 2016.5. From the cumulative slip distribution, we found that its shape spread in the dip direction and obtained a maximum slip of approximately 10.6 cm, a moment release of 2.7×10^{19} Nm, and an equivalent moment magnitude of 6.9. Comparing our results with the L-SSE that occurred in the Tokai region between 2000 and 2005, we found that the slip initiation location was almost the same, but the subsequent slip location was more southerly for the 2012–2016 Tokai L-SSE. Additionally, the maximum slip velocity and moment magnitude were smaller for the 2012–2016 L-SSE.

Keywords L-SSE, Tokai, Postseismic deformations, Inversion analysis, Spatiotemporal slip distribution

*Correspondence:
Hiroki Kawabata
222s410s@gsuite.kobe-u.ac.jp
Full list of author information is available at the end of the article

Introduction

In the Tokai region, central Japan, the Philippine Sea (PHS) plate is subducting beneath the Amurian plate along the Suruga Trough at convergence rates of 5.4–5.6 cm/year in a northwesterly direction [DeMets et al. 2010] (Fig. 1). Aseismic slips, called long-term slow slip events (L-SSEs), with durations of months to years, have occurred on the plate boundary in the Tokai region. Such aseismic slow slip events have been detected by the GNSS continuous observation system [GEONET (GNSS Earth Observation Network System)], which was launched by the Geospatial Information Authority of Japan in 1996.

L-SSEs occurred in the Tokai region from 2000 to 2005 [e.g., Ozawa et al. 2002; Ohta et al. 2004; Miyazaki et al. 2006; Liu et al. 2010; Ochi and Kato 2013; Ozawa et al. 2016]. Liu et al. (2010) estimated the slip distribution every 60 days using a Kalman filter-based network inversion method with an analysis period from 1998 to 2004.67. The slip occurred near Lake Hamana from the end of 2000 to 2001, followed by a slight northeastward shift of the slip area from late 2001. The slip weakened in late 2002. In early 2003, slip activity occurred again on the north side of Lake Hamana, and the slip reached a maximum in early 2004. The maximum amount of total slip was estimated to be approximately 24 cm, the maximum slip velocity was approximately 10 cm/year, and the equivalent moment magnitude (Mw) was approximately 7.0. Ochi and Kato (2013) inverted statically temporal changes to interplate coupling and long-term aseismic slip in the Tokai region from July 1996 to June 2009 by using continuous GNSS and levelling data. Then, using a new interpretation, they suggested that the interplate coupling and the aseismic slip should be inferred and compared with reference to a state of no coupling on the plate interface. As a result, slip appeared at a depth of approximately 25 km beneath northwestern Lake Hamana.

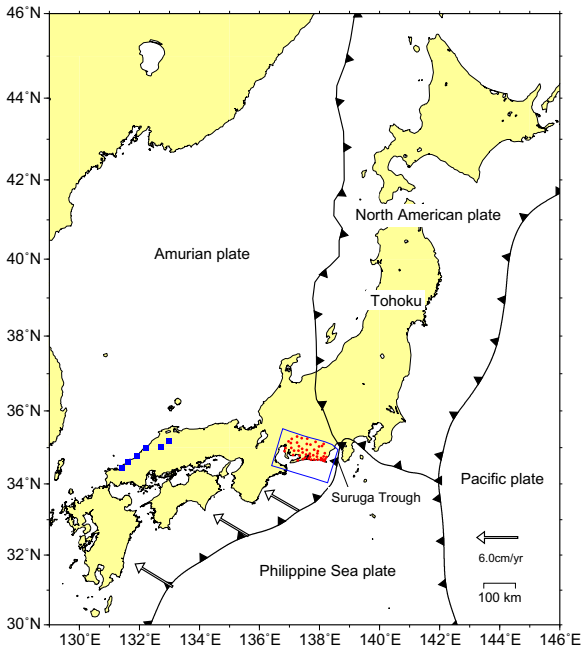

Fig. 1 Tectonic map in and around the Japanese Islands. The black line represents the plate boundary obtained by Bird (2003), Lindquist et al. (2004), and Iwasaki et al. (2015), and the solid triangles indicate the direction of motion of the plate to be subducted. The red circles and blue squares represent the GNSS observation stations and the reference stations used in this study, respectively. The blue box represents the horizontal projection of the model source region used in this study

According to Ozawa et al. (2016), the Tokai L-SSE occurred from 2013 to 2015. They showed the yearly slip distribution of the L-SSE using the time-dependent inversion method. The analytical period was from 1 January 2013 to 25 October 2015. The slip velocity was estimated to be 1–2 cm/year, and the location of the maximum slip area was almost the same in each period. Cumulative slip was estimated to be greater than 4 cm, with Mw6.6. However, the moment release rate was almost constant in their analysis, indicating that the L-SSE had not yet been completed in October 2015, and its whole rupture process had not yet been revealed. Therefore, we extended the time series data to be analyzed and concluded that the L-SSE had continued by the end of 2016, as described later in more detail. Additionally, although Ozawa et al. (2016) performed an inversion every 3 days, if we consider the noise level of the GNSS time series data, which is described in detail in a later section, it is impossible to discuss the difference in slip associated with the L-SSE during such a short period of time. For this reason, we suggest that they showed the inverted slip distributions on a map with a 1-year time window to take the conservative view. In this paper, to obtain meaningful inverted spatiotemporal slip distributions, we suggest that data with better signal-to-noise ratios should be used.

Therefore, in this study, we estimate the minimum time window for which signal-to-noise (S/N) ratios at almost all of the GNSS stations were carefully selected. More concretely, we set the time window as 0.5 years so that averages of S/N ratios of total used data both in north–south and east–west components can be larger than 1.0, excluding time windows with rather poor S/N ratios at the beginning and end of the whole analysis period. Thus, we aim to increase the temporal resolution of the rupture process of a single L-SSE as much as possible in a strict sense.

Using an inversion analysis of GNSS data with a time window of 0.1 year, Yoshioka et al. (2015) compared the rupture processes of the 1997–1998, 2002–2004, and 2009–2011 L-SSEs that occurred beneath the Bungo

Channel, southwest Japan, where L-SSEs have occurred repeatedly with recurrence intervals of 6–7 years. They showed that spatiotemporal slip distributions are different between them, although the final slip distributions are similar. Assuming the same time window of 0.1 year, Seshimo and Yoshioka (2022) investigated the most recent 2018–2019 Bungo Channel L-SSE and found that the rupture process was similar to that of the 2002–2004 Bungo Channel L-SSE. Therefore, it is important and meaningful to obtain the temporal evolution of a single L-SSE to identify its rupture process using the same inversion method by increasing the temporal resolution as much as possible.

Therefore, in this study, we estimate the spatiotemporal slip distributions associated with the 2012–2016 Tokai L-SSE after determining the minimum signal-to-noise ratio of the displacement data, thereby setting the minimum period of the time window to be carefully used for the inversion analysis by our own inversion method developed by Yoshioka et al. (2015). The results were then compared with those of previous studies for the L-SSE. We also compared the results obtained in this study with the previous 2000–2005 L-SSE that occurred in the Tokai region. In addition, we investigated the relationship between the occurrence of slip and tectonic tremors.

For GNSS time series analysis, inversion method, and model setup, please refer to Additional file 1: Texts S1, S2, and S3, respectively.

Results

Crustal deformations associated with the 2012–2016 Tokai L-SSE

Figures 2a and b show the horizontal and vertical displacement fields, respectively, at the GNSS stations in Fig. 3 for the total period of 2012.0–2018.0. Taking reference stations at six stations in the Chugoku district, southwest Japan shown in Fig. 1, the displacement fields were obtained, after removing the common-mode errors, the coseismic steps and the steps caused by antenna exchange, linear trend, annual and semiannual variations, and postseismic deformations associated with the 2011 Mw9.0 Tohoku-oki earthquake. For details, please see Additional file 1: Text S1. In the horizontal displacement field, the stations located other than in and around Omaezaki showed displacement in the south–southeast to southeast directions, whereas the stations located in and around Omaezaki showed displacement in the southeast to east directions. In the vertical displacement field, uplift was observed at stations located to the east to northeast of Lake Hamana, and subsidence was observed in the western part of Aichi Prefecture and Omaezaki, although subsidence near Omaezaki consists of both uplift periods and subsidence ones as explained later. In order to remove postseismic deformation associated with the 2011 Tohoku-oki earthquake, we used the similar method as Ozawa et al. (2016), resulting in similar dominant subsidence in the western part of Aichi Prefecture. They also tested simultaneous spatiotemporal slip inversion, assuming that postseismic deformation was caused by afterslip on the plate interface of the upper surface of the Pacific plate in northeast Japan. This removal method of the postseismic deformation also shows subsidence in the western part of Aichi Prefecture in their analysis. Therefore, we consider that subsidence in the western part of Aichi Prefecture is robust, regardless of the correcting method of the postseismic deformation.

Next, we focus on the temporal changes and describe their characteristics. Among the corrected time series data at the stations used in the analysis, Fig. 4b shows

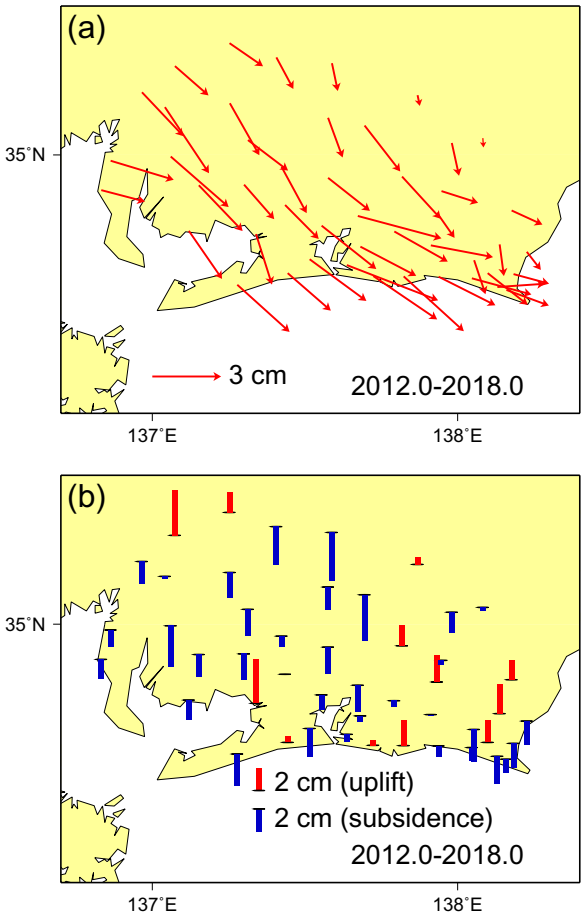

Fig. 2 Accumulated displacements associated with the L-SSE from 2012.0 to 2018.0 relative to the secular motion from 2008.0 to 2011.0. **a** Horizontal displacement field. **b** Vertical displacement field. The black horizontal line represents the location of the observation station. The red and blue bars represent uplift and subsidence, respectively

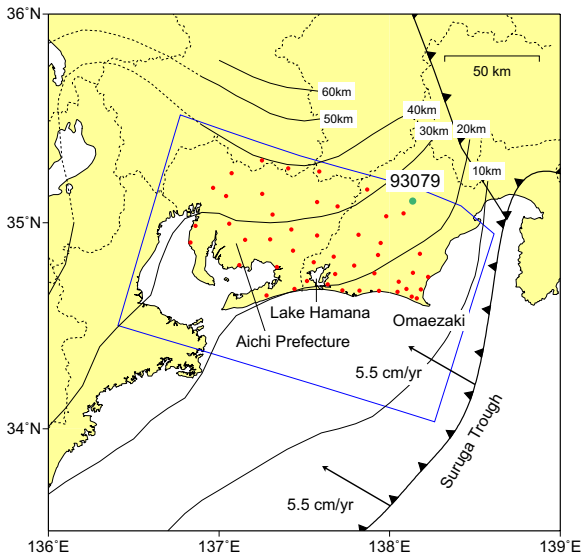

Fig. 3 Tectonic map in and around the Tokai region. The black lines indicate the plate boundaries obtained by Bird (2003), Lindquist et al. (2004), and Iwasaki et al. (2015), and the triangles indicate the direction of motion of the plate to be subducted. The black arrows are plate motion velocity vectors of the Philippine Sea (PHS) plate with respect to the Amurian plate at the Suruga Trough (DeMets et al. 2010). The black isodepth contour lines with an interval of 10 km represent the upper surface of the subducting PHS plate obtained by Hirose et al. (2008). The black dashed lines represent prefectural boundaries. The red solid circles represent the GNSS observation stations used in this study. The time series data at Station 93079 is shown in Additional file 1: Fig. S1. The blue box represents the horizontal projection of the model source region that allows slips on the plate boundary

the time series data of the three components at 10 stations around Lake Hamana (Fig. 4a). For the north–south component, gradual southward displacement began to be identified at most of the stations from the middle of 2012 and continued until the end of 2016. For the east–west component, eastward displacement was observed at Stations 071161, 041136, and 93050 from the middle of 2012. At Stations 970821, 93097, and 93098, eastward displacement was identified from the beginning of 2013. Each of the displacements ceased by the end of 2015. With respect to the vertical component, uplift was identified at Station 041136 from the middle of 2013 to the middle of 2014. Subsidence was observed at Stations 041136, 93050, and 970821 from the middle of 2014 to the end of 2014. The maximum displacements of the north–south and east–west components among 10 stations shown in Fig. 4 were approximately 2.4 cm to the south and approximately 4.0 cm to the east, respectively, and the maximum uplift was approximately 2.2 cm.

Horizontal displacements divided by 0.5 years for the total analytical period are shown in Fig. 5. From 2012.5 to 2013.0 (Fig. 5b), displacements in the southeast direction began to be observed at stations on the west to northwest side of Lake Hamana and in the east–southeast direction at stations on its east side. The directions of displacements changed to south–southeast at the stations on the west side of Lake Hamana and to east–southeast at the stations on its east side over time, and the displacements were larger at the stations on the east side than on the west side (Fig. 5c–e). After the displacements decreased (Fig. 5f), displacements in the south–southeast direction were observed again at many stations (Fig. 5g–j). It should be noted that the horizontal displacements associated with the L-SSE appear to have continued even in 2016, and displacements were smaller than standard errors at most of the stations in 2017 (Fig. 5k–l). This indicates that the L-SSE had finished around the end of 2016.

Vertical displacements divided by 0.5 years for the total analytical period are shown in Fig. 6. Uplift began to be observed at stations around Lake Hamana for the period of 2013.0–2013.5 (Fig. 6c), and larger uplift was observed on its east side for 2013.5–2014.0 (Fig. 6d), with the maximum uplift during this period being approximately 1.0 cm. Thereafter, the displacement decreased, and more stations showed subsidence (Fig. 6f). In the period of 2015.0–2015.5 (Fig. 6g), uplift was again observed at stations around Lake Hamana, and later uplift became larger at stations to the east of Lake Hamana. Subsidence was dominant near Omaezaki during the total analysis period. However, it should be noted that the subsidence consists of both uplift periods (Fig. 6d, h, j and k) and subsidence periods (Fig. 6b, e, f, i and l). Generally, the standard errors of the vertical displacements were 3 to 4 times larger than those of the horizontal displacements.

Judging from spatiotemporal horizontal displacement fields in Fig. 5, which are reliable than spatiotemporal vertical displacement fields which have larger standard errors (Fig. 6), it would be suitable to conclude that the L-SSE initiated in 2012.5–2013.0 and ended in 2016.5–2017.0, indicating that total period of the L-SSE was approximately 4.5 years.

Spatiotemporal slip distribution of the 2012–2016 Tokai L-SSE

Inversion analysis of the spatiotemporal slip distribution on the plate boundary with 3D geometry was performed using the data of horizontal displacements (Fig. 5) and vertical displacements (Fig. 6) at 0.5-year time windows at all the stations, which were corrected through the data analysis method.

We show the inverted slip distributions in Fig. 7. The slip in the southeast direction began to be identified on the southwest side of Lake Hamana for the period of 2013.0–2013.5 (Fig. 7c) and expanded, moved slightly

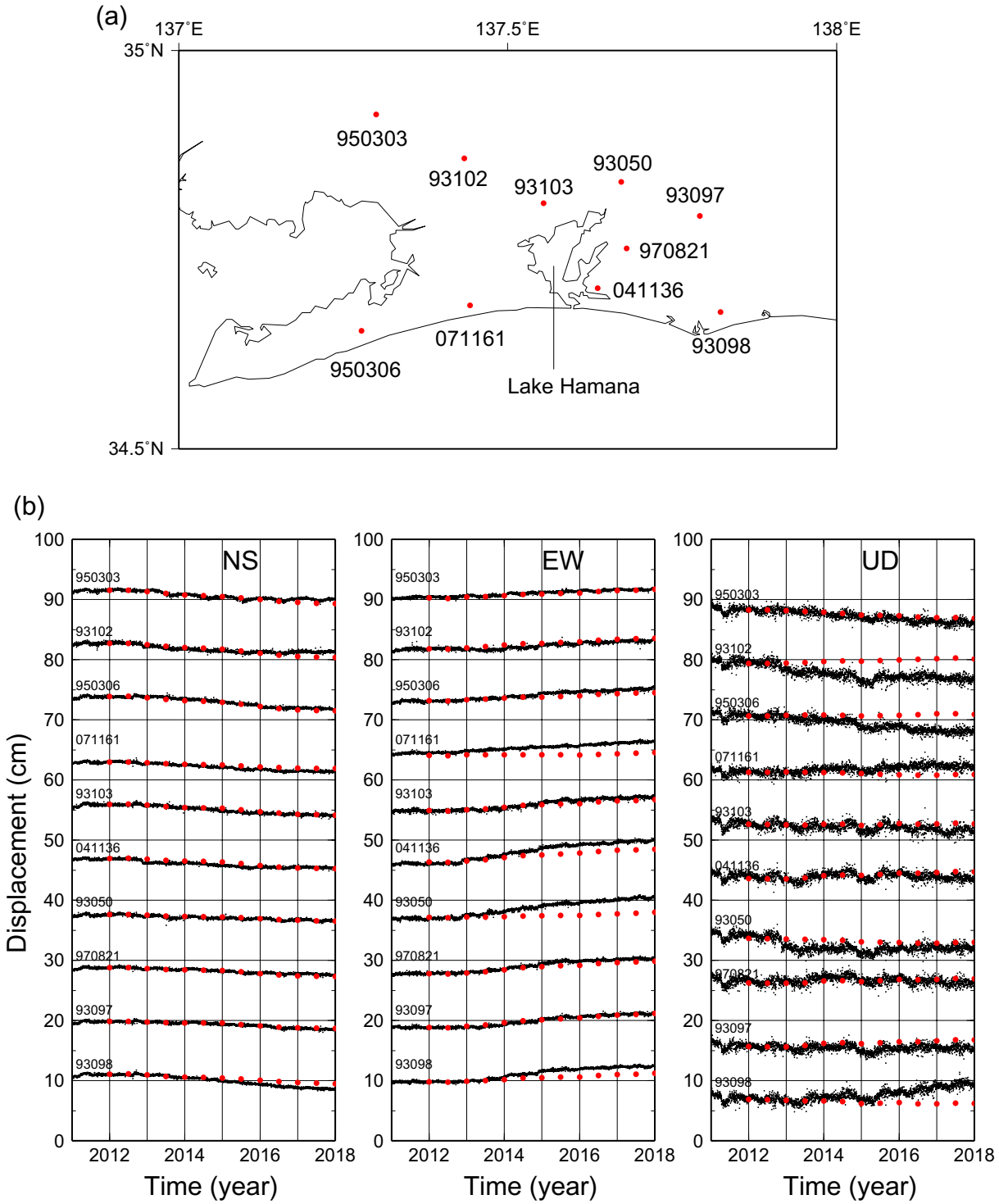

Fig. 4 **a** Locations of 10 GNSS observation stations for the time series data shown in (**b**). **b** GNSS time series data, including displacements associated with long-term slow slip events (L-SSEs) at the 10 observation stations shown in (**a**). The black dots indicate daily data after removing coseismic steps, steps caused by antenna exchange, linear trends, annual and semiannual variations, common-mode errors, and postseismic deformation. The period of the linear trends is taken from 1 January 2008 to 31 December 2010, before the occurrence of the 2011 Tohoku-oki earthquake. For details, please see Additional file 1: Text S1. The red circles represent the displacement at each component at each observation station every 0.5 years, which are calculated from the spatiotemporal slip distribution shown in Fig. 7. Left: North—south component. Center: East—west component. Right: Up–down component

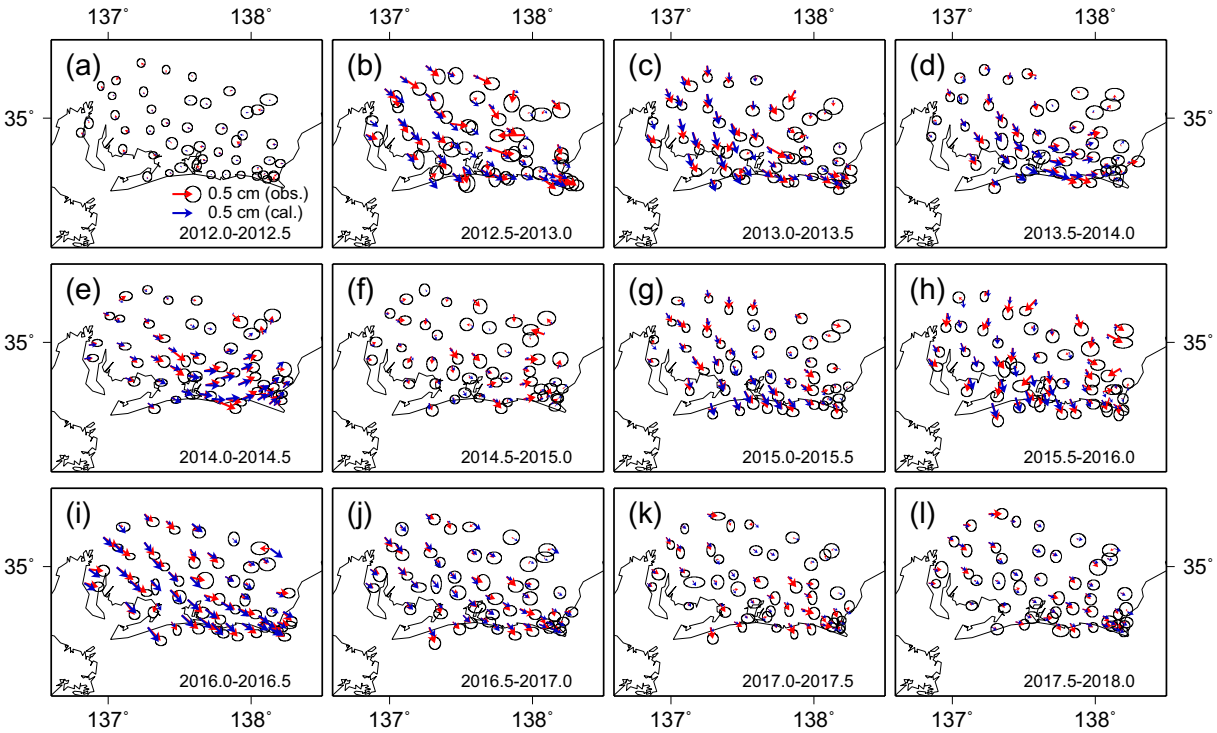

Fig. 5 Spatial distribution of horizontal displacement associated with the L-SSE in every 0.5-year time window from 2012.0 to 2018.0. The red arrows represent horizontal displacement vectors obtained from time series data after various corrections. The ellipse at the tip of the arrow represents the 1σ error ellipse. The blue arrows denote horizontal displacement vectors calculated from the inverted slip distributions shown in Fig. 7. **a** 2012.0–2012.5. **b** 2012.5–2013.0. **c** 2013.0–2013.5. **d** 2013.5–2014.0. **e** 2014.0–2014.5. **f** 2014.5–2015.0. **g** 2015.0–2015.5. **h** 2015.5–2016.0. **i** 2016.0–2016.5. **j** 2016.5–2017.0. **k** 2017.0–2017.5. **l** 2017.5–2018.0

northeastward, and the slip became the largest during the period of 2013.5–2014.0 (Fig. 7d). At this time, the maximum slip velocity was estimated to be approximately 3.5 cm/year. The slip was oriented in the southeast direction. A slip area of more than 1 cm for each time window was found on the western side of Lake Hamana during the period of 2013.0–2014.5 (Fig. 7c–e). The slip directions appear to have changed slightly during that period, reflecting the directional changes in horizontal displacement fields during that period (Fig. 5c–e). During the period of 2014.5–2015.0 (Fig. 7f), the slip beneath Lake Hamana weakened and became active again on the west side of Lake Hamana in the subsequent period (Fig. 7g), continued, and expanded there (Fig. 7h–i). If we define a subevent as slippage larger than 1 cm, these results indicate that the L-SSE consisted of two subevents. The slip continued until the end of 2016 (Fig. 7j). Slips almost ceased in 2017.0–2017.5 (Fig. 7k), which is consistent with the observed smaller horizontal and vertical displacements in the corresponding time windows (Figs. 5k and 6k) than those in the previous time windows.

The spatial distribution of the total amount of slip in the Tokai L-SSE from 2012.0 to 2018.0 is shown in Fig. 8. The maximum slip area was located at a depth of approximately 20 km, and the areas with slips greater than 2 cm were located at depths between approximately 15 km and 33 km. The maximum amount of total slip was estimated to be approximately 10.6 cm, with a moment release of 2.7×10^{19} Nm and Mw6.9.

As for comparison between observed and calculated displacement fields, please refer to Additional file 1: Text S4.

Incidentally, we tested the case where time window is 0.25 years, which is a half of the above time window (Additional file 1: Figs. S1, S2 and S3). In this case, S/N ratios of horizontal displacements became much worse: Horizontal displacement vectors are less than standard errors at almost all the stations at all the time windows. Although average of S/N ratios of all the vertical displacements for time window of 0.5 years is about 0.5, the values became much worse of about 0.25. As a result of the inversion analysis, statistically meaningful southeastward slips, which are larger than estimation errors of 1σ, can be only identified around from 2014.0 to 2015.5. However, we cannot distinguish difference between no slips and discernible slips, both of the slip amounts are

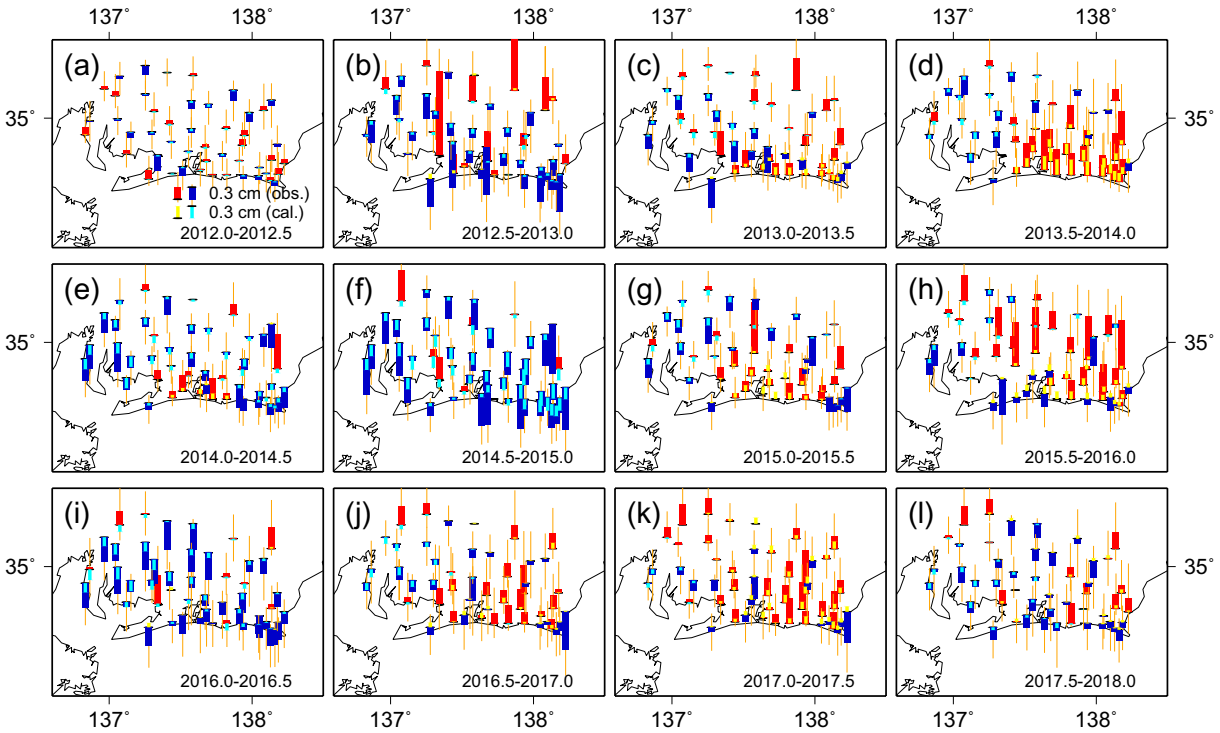

Fig. 6 Spatial distribution of the vertical displacement associated with the L-SSE in every 0.5-year time window from 2012.0 to 2018.0. The short horizontal black line represents the location of the observation station. The thick red and blue bars above and below the horizontal line represent the observed uplift and subsidence, respectively, derived from the time series data after various corrections. The orange bars at the tips of the red and blue bars represent the ± 1σ error. The thin yellow and light blue bars above and below the horizontal line denote uplift and subsidence, respectively, calculated from the inverted slip distributions shown in Fig. 7. Periods (**a**–**l**) are the same as those in Fig. 5

less than estimation errors of 1σ for the rest of the time windows. Although we admit that it is difficult to connect S/N ratios of the horizontal and vertical displacements with statistically meaningful inverted spatiotemporal slip distributions directly, determining a minimum time window so that the averages of S/N ratios of both NS and EW components can be larger than 1.0 may be one of the useful measures to obtain statistically meaningful spatiotemporal slip distributions for which most of the slip amounts are larger than estimation errors of 1σ.

Discussion

Comparison with previous studies in the Tokai region

An L-SSE occurred in the Tokai region from 2000 to 2005 [e.g., Ozawa et al. 2002; Ohta et al. 2004; Miyazaki et al. 2006; Liu et al. 2010; Ochi and Kato 2013; Ozawa et al. 2016]. Here, we compare the results obtained in this study with those in the most recent of these papers, i.e., Ozawa et al. (2016). According to their paper, slip initiated on the southwest side of Lake Hamana in 2001. In 2002, slip was no longer observed on the southwest side of Lake Hamana, but slip was observed on the north side of Lake Hamana; then, in 2003, slip expanded on the north side of Lake Hamana. In 2004, the slip area expanded in a southwesterly direction, but this was considered to be due to the 2004 Kii-hanto-nanto-oki earthquake (Mw7.3) that occurred at the upper surface of the Philippine Sea (PHS) plate, and this southwesterly expansion of the slip area was considered unreliable. In 2005, the slip weakened, and in 2006, no slip was observed around Lake Hamana. The moment magnitude was estimated to be greater than 7.0.

A comparison with the slip distribution of the 2012–2016 Tokai L-SSE estimated in this study reveals consistency with the slip that initiated in the southwestern part of Lake Hamana. The 2000–2005 Tokai L-SSE subsequently caused slip on the north side of Lake Hamana, while the 2012–2016 Tokai L-SSE caused slip around Lake Hamana, indicating that the latter was more southerly than the former (Fig. 8). The other difference between them is the difference in the equivalent moment magnitude: the Mw of the 2012–2016 Tokai L-SSE was smaller than that of the 2000–2005 Tokai L-SSE (Table 1).

We also compared the spatiotemporal slip distribution associated with the 2012–2016 Tokai L-SSE obtained in this study with those by Ozawa et al. (2016) and Sakaue

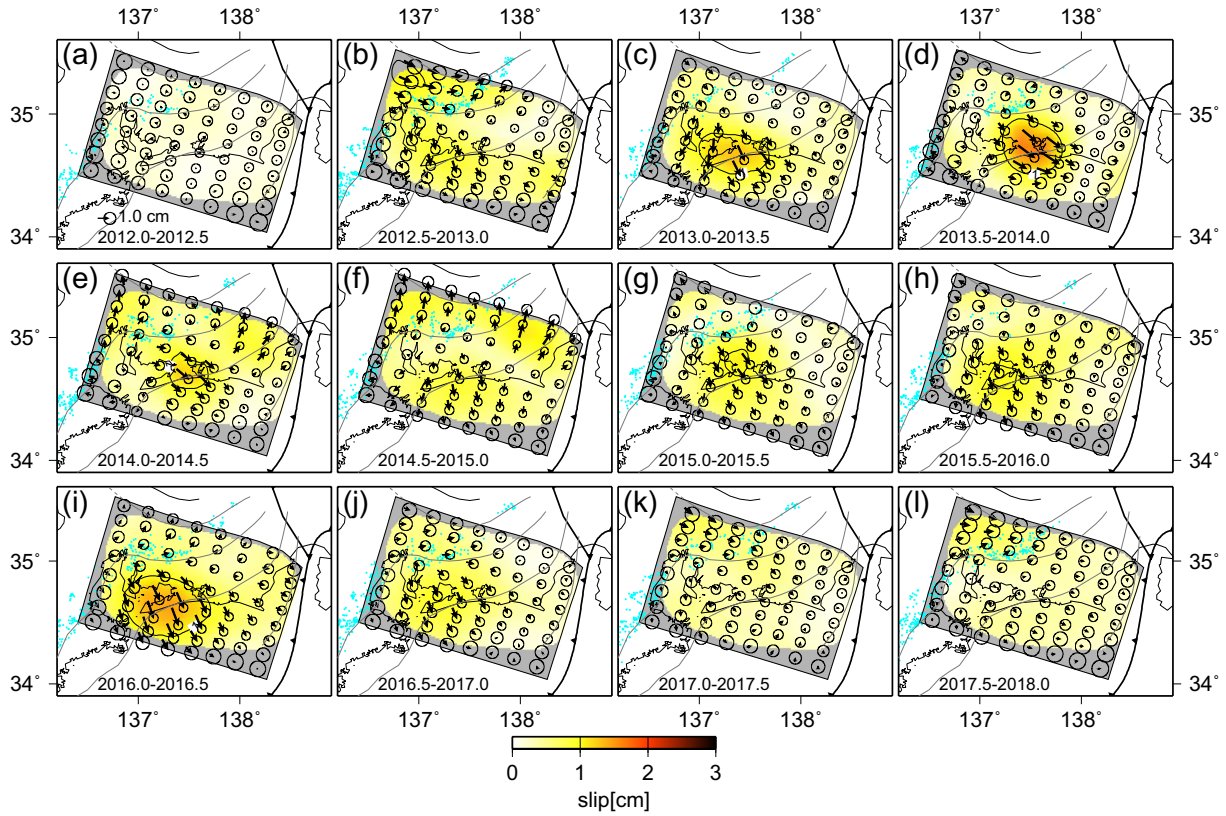

Fig. 7 Spatiotemporal slip distribution associated with the 2012–2016 Tokai L-SSE inverted from the horizontal and vertical displacement data shown in Figs. 5 and 6, respectively, with a 0.5-year time window from 2012.0 to 2018.0. The arrows indicate the direction and amount of slip on the continental upper plate relative to the oceanic lower plate at the plate boundary, and the circles at the tips of the arrows indicate the estimation error of 1σ. The contour lines represent the amount of slip, with an interval of 1 cm. The gray area represents the area where the resolution is less than 0.05. The thin gray isodepth contour lines with an interval of 10 km represent the upper surface of the subducting PHS plate obtained by Hirose et al. (2008). The black line represents the plate boundary obtained by Bird (2003), Lindquist et al. (2004), and Iwasaki et al. (2015), and the solid triangles indicate the direction of motion of the plate to be subducted. The light blue dots represent the epicenters of tectonic tremors that occurred within the period of each time window. Periods (**a**) to (**l**) are the same as those in Fig. 5

et al. (2019). Ozawa et al. (2016) used the network filter inversion by McGuire and Segall (2003) to estimate the slip distribution by performing the analysis for the period from 1 January 2013 to 25 October 2015. The exact start date is unknown, but they state that the slip occurred around Lake Hamana at the beginning of 2013 at the latest. In the period from 1 January 2013 to 1 January 2014, slip was identified on the southwest side of Lake Hamana, followed by an expansion of slip in the following year. From 1 January 2015 to 25 October 2015, the slip area greater than 1 cm moved 10–20 km to the west. The maximum slip area did not move significantly. The total amount of slip was estimated to be more than 4 cm and was estimated to be Mw6.6 during the above analytical period.

Sakaue et al. (2019) analyzed GNSS data from 1 January 2008 to 31 January 2016 for the Tokai region, in order to study long- and short-term SSEs on the subduction interface. The dataset included their new temporary stations to obtain high spatial resolution observations. They applied a time-dependent inversion with improved temporal resolution to GNSS data and obtained the spatiotemporal evolution of long- and short-term SSEs. Their results show the very slow and stable slip of the L-SSE with Mw6.6, reaching amount of slip less than 6 cm. However, since temporal change of slip patterns is not shown associated with the L-SSE, it would be difficult to make a direct comparison between their slip time evolution and ours.

The slip location obtained in this study was consistent with that of Ozawa et al. (2016). However, because we extended the analytical period before and after that of Ozawa et al. (2016) to 2012.0–2018.0 and used a minimum time window of 0.5 years, which was determined by taking into account the signal-to-noise ratio of the observed displacement in each time window, we clarified the timing of the initiation and end of slippage to be 2012.5 and 2017.0, respectively. Therefore, the duration

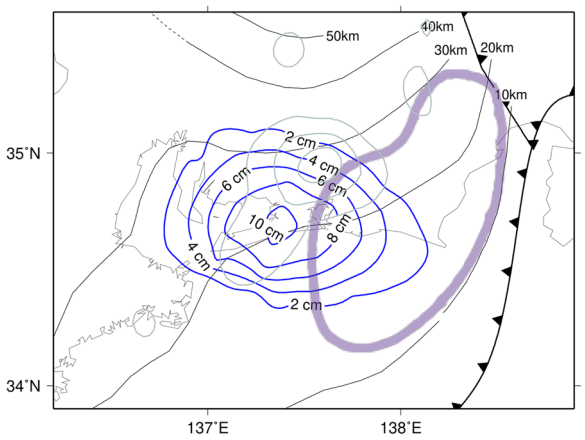

Fig. 8 The blue contour lines represent spatial distribution of the total amount of slip of the Tokai L-SSE from 2012.0 to 2018.0. The contour interval is 2 cm. The gray contours show the slip magnitude of the previous Tokai L-SSE for the period between 1 January 2001 and 1 January 2008, with a contour interval of 10 cm by Ozawa et al. (2016). The area surrounded by the thick purple line is the source region of the anticipated Tokai megathrust earthquake, which was proposed by the Central Disaster Prevention Council of the Cabinet Office, Government of Japan (2001). The black isodepth contour lines with an interval of 10 km represent the upper surface of the subducting Philippine Sea plate obtained by Hirose et al. (2008). The black line represents the plate boundary obtained by Bird (2003), Lindquist et al. (2004), and Iwasaki et al. (2015), and the solid triangles indicate the direction of motion of the plate to be subducted

of the L-SSE was estimated to be 4.5 years, which was much longer than the period of less than 3 years proposed by Ozawa et al. (2016). As a natural consequence, the total slip amount and equivalent moment magnitude were obtained as 10.6 cm and 6.9, respectively, which were much larger than the values of 4 cm and 6.6 estimated by Ozawa et al. (2016) (Table 2). The total slip distribution spread with an oval shape in the east–southeast to west–northwest direction (Fig. 8), which was opposite to the spreading in the northeast to southwest direction of Ozawa et al. (2016). We also identified that the L-SSE consisted of two subevents. The first subevent initiated on the southwest side of Lake Hamana, and the slip expanded during 2013.0–2014.5 (Fig. 7c–e). The second subevent took place approximately 20 km west of the slip area of the first subevent during 2015.0–2016.5 (Fig. 7g–i).

Table 2 The differences between the results of Ozawa et al. (2016) and this study

	Ozawa et al. (2016)	This study
Analytical period	1 January 2013 to 25 October 2015	1 January 2012 to 31 December 2017
Timing of the onset of slip	Beginning of 2013	2012.5–2013.0
Total amount of slip	Less than 6 cm	10.6 cm
Equivalent moment magnitude	Mw6.6	Mw6.9

Tectonic implication of the 2012–2016 Tokai L-SSE

By analyzing GNSS data in the Tokai region from January 2001 to December 2002, Ohta et al. (2004) estimated the slip distribution of the L-SSE that occurred during that period. They stated that tectonic tremors occurred on the downdip side of the L-SSE and that there is a correlation between the L-SSE and tectonic tremors. The relationship between tectonic tremors and an L-SSE has been pointed out not only in the Tokai region but also in other regions. For example, Seshimo and Yoshioka (2022) stated that the number of tectonic tremors increased in the 2018–2019 Bungo Channel L-SSE when the slip of the L-SSE was large for each time window of 0.1 year.

In Fig. 7, we also plot the tectonic tremors that occurred along with the slip distribution estimated for each time window. However, it is difficult to identify the relationship between the slip amount and occurrence of tectonic tremors for the 2012–2016 L-SSE. Although tectonic tremors appear to be activated at the downdip side of the L-SSE in Fig. 7d, more intense activated tectonic tremors take place nearly at the same locations in Fig. 7b and l, for which little slips associated with the L-SSE can be identified at their updip sides. Tectonic tremors were not activated in this L-SSE due to the small moment release and the slip amount per unit time. This may also be because the slip region was far from the area where the tectonic tremors took place.

Table 1 The differences between the results of the 2000–2005 Tokai L-SSE [Ozawa et al. (2016)] and 2012–2016 Tokai L-SSE (this study)

	2000–2005 Tokai L-SSE [Ozawa et al. (2016)]	2012–2016 Tokai L-SSE [This study]
Maximum slip velocity	More than 10 cm/year	3.5 cm/year
Equivalent moment magnitude	Greater than Mw7.0	Mw6.9
Duration	Approximately 5 years	Approximately 4.5 years

Kodaira et al. (2004) found regions with high pore-water pressure in the oceanic crust in subducted seamounts and their deep extensions through high-precision seismic reflection surveys in the Tokai region along the across-arc profile. They argued that the expansion of the conditionally stable slip region was the cause of the 2000–2005 L-SSE in that location. However, since the main slip area of the 2012–2016 L-SSE is located southwestward of the previous event and spreads in the updip and downdip directions, it may occur at the transition zone from conditionally stable slip to unstable slip. Kato et al. (2010) revealed the seismic velocity structure using seismic tomography and receiver function analysis in the Tokai region along the across-arc direction. Based on their velocity structure, they suggested that overpressured fluids in the 2000–2005 L-SSE occurrence region appear to be trapped within the oceanic crust by an impermeable cap rock in the fore-arc and impede intraslab earthquakes therein. However, their profile passes through eastern Omaezaki, and there is no overlap with the slip area obtained in this study; thus, it would be difficult to make a direct comparison between them.

Performing 2D thermal modeling associated with subduction of the PHS plate, Suenega et al. (2016) estimated the temperature distribution on the plate interface in the Tokai region. They showed that the temperatures of the upper surface of the PHS plate, where the 2000–2005 Tokai L-SSE occurred, were estimated to be 350–450 °C for the isoslip line where the cumulative slip was 10 cm in Miyazaki et al. (2006). If we take the depth range of total slip greater than 5 cm, which is approximately half of the maximum amount of slip (Fig. 8), its temperature ranges from approximately 300 to 420 °C. It should be noted that if we take the isoslip line of the cumulative slip of 10 cm obtained in this study, its updip limit almost coincides with the temperature of 350 °C. The updip limit temperature of 350 °C for an L-SSE was also consistent with the 1997, 2003, and 2010 Bungo Chanel L-SSEs that occurred in southwest Japan (Nakata et al. 2017; Ji et al. 2016). According to Hyndman et al. (1997), this temperature range is located at the downdip end of the coseismic slip area, corresponding to the brittle–ductile and unstable to stable sliding transition zone.

In the Tokai region, megathrust earthquakes have occurred repeatedly, with recurrence intervals of approximately 150 years (e.g., Kumagai 1996). The most recent event was the 1854 Ansei earthquake (M8.4). Thus, the region has been a so-called seismic gap for almost 170 years, and the next megathrust earthquake will likely take place in the Tokai region in the near future (e.g., Ishibashi 1981). In Fig. 8, we show the source region of the anticipated megathrust earthquake proposed by the Central Disaster Prevention Council of the Cabinet Office, Government of Japan (2001) (https://www.bousai.go.jp/jishin/tokai/senmon/11/pdf/siryou2-2.pdf). If we compare it with the slip distribution of the L-SSE obtained in this study, we notice that the downdip limit of the former almost coincides with the maximum slip area of the latter. This may suggest that the slip of the L-SSE took place not only in the brittle–ductile transition zone but also in the downdip portion of the brittle zone, indicating invasion of the coupled area by slip associated with the L-SSE. This situation may be similar to the Guerrero seismic gap in the Mexico subduction zone along the Middle American Trench, which has been active for more than 110 years (Kostoglodov and Pacheco 1999) and where large L-SSEs may have invaded a deeper part of the strongly coupled seismogenic zone (e.g., Yoshioka et al. 2004).

In order to identify causal relationship between the L-SSE and the anticipated Tokai earthquake more quantitatively, we calculated Coulomb stress change (Coulomb Failure Function: Δ CFF) for the source area of the Tokai earthquake when total slip distribution of the L-SSE was given, using Okada (1992)'s plane fault model. Therefore, we approximated the 3-D plate geometry with a flat fault plane, whose strike and dip were determined from the range of the L-SSE slip distribution and the isodepth contour lines of the upper surface of the PHS plate. Since the Tokai earthquake is assumed to occur in a shallow area on the same plate boundary as the L-SSE, we assumed that the source region of the Tokai earthquake is located on the same flat fault plane as that of the L-SSE occurrence. Furthermore, at the time of the Tokai earthquake, we also assumed that the continental Amurian plate would slip in the opposite direction of subduction direction of the PHS plate with respect to the Amurian plate by DeMets et al. (2010). Specifically, the strike, dip, and rake of the fault plane of the L-SSE and the Tokai earthquake were set to 270.0°, 12.7°, and 148.7°, respectively. Then, based on the total slip distribution shown in Fig. 8, we divided the L-SSE slip area into multiple subfaults and gave different slip amounts to each subfault to calculate Δ CFF for the source area of the Tokai earthquake, assuming that the value of the apparent friction coefficient μ' was 0.4 (e.g., King et al. 1994).

Figure 9 shows thus calculated spatial distribution of Δ CFF. In the slip area of the L-SSE and approximately two thirds of the deeper source area of the Tokai earthquake, the value of Δ CFF became negative. However, for the rest of one third of the shallow Tokai earthquake source region, Δ CFF shows positive values ranging from 0.00 MPa to 0.005 MPa, indicating a sense that promotes the occurrence of the Tokai earthquake.

Kimura and Kakehi (2005) showed that the aftershocks of the Hyogo-ken Hokubu earthquake (Mw5.2) that

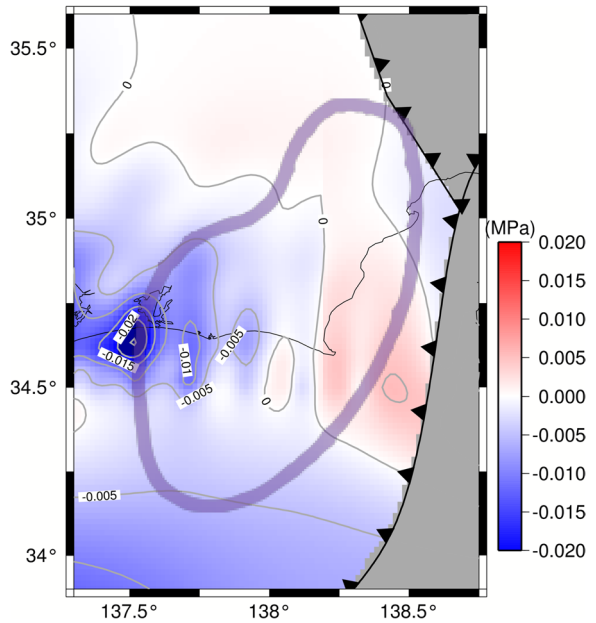

Fig. 9 Horizontal projection of spatial distribution of Δ CFF caused by the total slip distribution associated with the L-SSE (Fig. 8) to calculate its effect on the anticipated Tokai earthquake on the same flat fault plane. For details, please see the text. The red and blue areas denote positive and negative values of Δ CFF, respectively

occurred in southwestern Japan in 2001 took place in areas where Δ CFF due to the slip of the mainshock was positive. From their results, there is a good correspondence between the Δ CFF increase area of about 0.01 MPa and the area where aftershocks occur.

Therefore, in the shallow source area of the Tokai earthquake, the analysis of Δ CFF indicates that the Tokai earthquake is accelerated by the occurrence of the L-SSE, but its value remains below approximately 0.005 MPa. Therefore, it is unlikely that this L-SSE had a major influence on the occurrence of the Tokai earthquake. This is because as the amount of slip due to the L-SSE gradually decreases spatially, and so, its spatial gradient, which is related to stress change, also decreases.

Conclusions

In this study, we used GNSS time series data to estimate the spatiotemporal slip distribution associated with the long-term slow slip event that occurred in the Tokai region from 2012 to 2016 through inversion analysis. The significant results obtained in this study are summarized as follows:

(1) In the horizontal displacement fields, southeastward displacements began to be observed on the west side of Lake Hamana around from 2012.5, and the directions of displacements changed over time to east–southeast at the stations. On the other hand, the directions of displacements changed over time from east–southeast to east at the stations on the east side of Lake Hamana. The amount of displacement became larger at the stations on the east side than on the west side over time. After the displacements decreased, south–southeast displacements were observed again at many stations. The horizontal displacements appeared to continue even in 2016, and the displacements were smaller than the standard errors at most of the stations in 2017. Therefore, we propose that the duration of the 2012–2016 Tokai L-SSE was 4.5 years, which is much longer than that estimated in a previous study. In the vertical displacement field, uplift was observed at stations around and on the east side of Lake Hamana. After the displacement increased, subsidence was observed once, but then uplift was observed again. Subsidence was dominant near Omaezaki in most of the time windows.

(2) The L-SSE consisted of two subevents. The first subevent occurred during the period from 2013.0 to 2014.5. The slip initiated on the southwest side of Lake Hamana, and it expanded on the plate boundary. Subsequently, the slip area moved slightly northeastward, the amount of slip reached its maximum, and the slip changed to the east–southeast direction. The second smaller subevent took place on the west side of Lake Hamana for 2015.0–2015.5.

(3) The maximum total amount of slip was estimated to be approximately 10.6 cm, the moment release was estimated to be 2.7×10^{19} Nm, with Mw6.9, and the maximum slip velocity was approximately 3.5 cm/year for the period of 2013.5–2014.0.

(4) The slip distribution spread in the dip direction. This suggests that the L-SSE occurred not only in the brittle–ductile transition zone but also in the downdip portion of the brittle strongly coupled zone.

(5) From the analysis using Δ CFF, although the L-SSE is a sense that promotes the occurrence of the anticipated Tokai earthquake on its shallow source region, its effect would be limited.

Abbreviations

GNSS	Global Navigation Satellite System
L-SSE	Long-term slow slip event
GSI	Geospatial Information Authority of Japan
NIED	National Research Institute for Earth Science and Disaster Prevention

Supplementary Information

The online version contains supplementary material available at https://doi.org/10.1186/s40562-023-00316-4.

Additional file 1. Text S1 GNSS time series data analysis. **Text S2** Inversion method. **Text S3** Model setup. **Text S4** Comparison between observed and calculated displacement fields. **Figure S1** Spatial distribution of horizontal displacement associated with the L-SSE in every 0.25-year time window from 2012.0 to 2018.0. **Figure S2** Spatial distribution of vertical displacement associated with the L-SSE in every 0.25-year time window from 2012.0 to 2018.0. **Figure S3** Spatiotemporal slip distribution associated with the 2012-2016 Tokai L-SSE inverted from the horizontal and vertical displacement data shown in Figs. S1 and S2, respectively, with a 0.25-year time window from 2012.0 to 2018.0. **Figure S4** Time series data from 2012.0 to 2018.0 at Station 93079 in Fig. 2. **Figure S5** Changes in the minimum value of ABIC, depending on times of inversions. **Table S1** Change in the values of $\hat{\alpha}$, $\hat{\beta}$ and $\hat{\gamma}$ at each time of inversions.

Acknowledgements
We thank T. Yabuki for sharing the original source codes of the slip inversion of Yabuki and Matsu'ura (1992). We also thank T. Kimura and Y. Kakehi for sharing the source code of ΔCFF, where ΔCFF is calculated from the strain field due to a shear fault (Okada, 1992). We are grateful to the Editor R. Y. Chuang, two anonymous reviewers, H. Hirose and S. Kita for their constructive comments to improve the manuscript. We used GNSS time series data from GEONET of the Geospatial Information Authority of Japan (GSI) and the tectonic tremor catalog of the National Research Institute for Earth Science and Disaster Prevention (NIED). We used the plate boundary model by Iwasaki et al. (2015), which was constructed from topography and bathymetry data by Geospatial Information Authority of Japan (250-m digital map), Japan Oceanographic Data Center (500m mesh bathymetry data, J-EGG500, http://www.jodc.go.jp/jodcweb/JDOSS/infoJEGG_j.html) and Geographic Information Network of Alaska, University of Alaska (Lindquist et al. 2004). Figures were created by using the Generic Mapping Tools (GMT) (version: GMT 4.5.7, URL link: https://www.generic-mapping-tools.org/download/) (Wessel and Smith 1998).

Author contributions
YS analyzed GNSS time series data, carried out the slip inversion, and wrote the paper. HK prepared and revised some of the figures and submitted the paper. SY organized and guided the study, pointed out possible problems with the study, advised about solutions, and edited the paper. FO-C pointed out possible problems with the study and advised about solutions.

Funding
This work was partly supported by a MEXT KAKENHI Grant [Grant Number 21H05203] and a Kobe University Strategic International Collaborative Research Grant (Type B Fostering Joint Research).

Availability of data and materials
In this study, we utilized the daily coordinate data of GNSS stations provided by the GSI (https://www.gsi.go.jp/ENGLISH/geonet_english.html), the electronic reference point maintenance work list (https://terras.gsi.go.jp/denshi_hosyu.php), NIED's hypocenter catalogue of tectonic tremors (https://hinetwww11.bosai.go.jp/auth/?LANG=en), Japan Oceanographic Data Center's 500 m mesh bathymetry data, J-EGG500 (http://www.jodc.go.jp/jodcweb/JDOSS/infoJEGG_j.html).

Declarations

Competing interests
The authors declare that they have no competing interest.

Author details
[1]Department of Planetology, Graduate School of Science, Kobe University, Rokkodai-cho 1-1, Nada ward, Kobe 657-8501, Japan. [2]Research Center for Urban Safety and Security, Kobe University, Rokkodai-cho 1-1, Nada ward, Kobe 657-8501, Japan. [3]Department of Geophysics, Faculty of Physical and Mathematical Sciences, University of Chile, Av. Blanco Encalada 2002, Santiago, Chile. [4]Data Observatory Foundation, ANID Technology Center No. DO210001, Santiago, Chile.

Received: 7 July 2023 Accepted: 5 December 2023
Published online: 21 December 2023

References

Bird P (2003) An updated digital model of plate boundaries. Geochem Geophys Geosyst 4(3):1027. https://doi.org/10.1029/2001GC000252
Central Disaster Prevention Council of the Cabinet Office, Government of Japan (2001). https://www.bousai.go.jp/jishin/tokai/senmon/11/pdf/siryou2-2.pdf. Accessed 11 Dec 2023
DeMets C, Gordon RG, Argus DF (2010) Geologically current plate motions. Geophys J Int 181:1–80
Hirose F, Nakajima J, Hasegawa A (2008) Three-dimensional seismic velocity structure and configuration of the Philippine Sea slab in southwestern Japan estimated by double-difference tomography. J Geophys Res Solid Earth 113:B09315. https://doi.org/10.1029/2007JB005274
Hyndman RD, Yamano M, Oleskevich DA (1997) The seismogenic zone of subduction thrust faults. Island Arc 6:244–260
Ishibashi K (1981) Specification of a soon-to-occur seismic faulting in the Tokai district central Japan based upon seismotectonics. In: Simpson DW, Richards PG (eds) Earthquake prediction, vol 4. Maurice Ewing series. American Geophysical Union, Washington, pp 297–332
Iwasaki T, Sato H, Shinohara M, Ishiyama T, Hashima A (2015) Fundamental structure model of island arcs and subducted plates in and around Japan. 2015 Fall Meeting, American Geophysical Union, San Francisco, 14–18 December 2015
Ji Y, Yoshioka S, Matsumoto T (2016) Three-dimensional numerical modeling of temperature and mantle flow fields associated with subduction of the Philippine Sea plate, southwest Japan. J Geophys Res Solid Earth. https://doi.org/10.1002/2016JB012912
Kato A, Iidaka T, Ikuta R, Yoshida Y, Katsumata K, Iwasaki T, Sakai S, Thurber C, Tsumura N, Yamaoka K, Watanabe T, Kunitomo T, Yamazaki F, Okubo N, Suzuki S, Hirata N (2010) Variations of fluid pressure within the subducting oceanic crust and slow earthquakes. Geophys Res Lett 37:L14310. https://doi.org/10.1029/2010GL043723
Kimura T, Kakehi Y (2005) Rupture process of the 2001 Hyogo-ken Hokubu, Japan, earthquake (Mw 5.2) and comparison between the aftershock activity and the static stress changes. Bull Seismol Soc Am 95:145–158. https://doi.org/10.1785/0120040012
King GCP, Stein RS, Lin J (1994) Static stress changes and the triggering of earthquakes. Bull Seismol Soc Am 84:935–953
Kodaira S, Iidaka T, Kato A, Park J-O, Iwasaki T, Kaneda Y (2004) High pore fluid pressure may cause silent slip in the Nankai Trough. Science 304:1295–1298
Kostoglodov V, Pacheco JF (1999) Cien Años de Sismicidad de Mexico, Poster Map, Inst de Geof, Univ Nac Auton Mex, Mexico City. http://usuarios.geofisica.unam.mx/vladimir/sismos/100a%F1os.html. Accessed 11 Dec 2023
Kumagai H (1996) Time sequence and the recurrence models for large earthquakes along the Nankai Trough revisited. Geophys Res Lett 23:1139–1142
Lindquist KG, Engle K, Stahlke D, Price E (2004) Global topography and bathymetry grid improves research efforts. Eos Trans 85(19):186. https://doi.org/10.1029/2004EO190003
Liu Z, Owen S, Dong D, Lundgren P, Webb F, Hetland E, Simons M (2010) Integration of transient strain event with models of plate coupling and areas of great earthquakes in southwest Japan. Geophys J Int 181:1292–1312. https://doi.org/10.1111/j.1365-246X.2010.04599.x
McGuire JJ, Segall P (2003) Imaging of aseismic slip transients recorded by dense geodetic networks. Geophys J Int 155:778–788
Miyazaki S, Segall P, McGuire JJ, Kato T, Hatanaka Y (2006) Spatial and temporal evolution of stress and slip rate during the 2000 Tokai slow earthquake. J Geophys Res 111:B03409. https://doi.org/10.1029/2004JB003426
Nakata R, Hino H, Kuwatani T, Yoshioka S, Okada M, Hori T (2017) Discontinuous boundaries of slow slip events beneath the Bungo Channel, southwest Japan. Sci Rep 7:6129. https://doi.org/10.1038/s41598-017-06185-0

Ochi T, Kato T (2013) Depth extent of the long-term slow slip event in the Tokai district, central Japan: a new insight. J Geophys Res 118:4847–4860. https://doi.org/10.1002/jgrb.50355
Ohta Y, Kimata F, Sagiya T (2004) Reexamination of the interplate coupling in the Tokai region, central Japan, based on the GPS data in 1997–2002. Geophys Res Lett 31:L24604. https://doi.org/10.1029/2004GL021404
Okada Y (1992) Internal deformation due to shear and tensile faults in a half-space. Bull Seismol Soc Am 82(2):1018–1040
Ozawa S, Murakami M, Kaidzu M, Tada T, Sagiya T, Hatanaka Y, Yarai H, Nishimura T (2002) Detection and monitoring of ongoing aseismic slip in the Tokai region, central Japan. Science 298:1009–1012
Ozawa S, Tobita M, Yarai H (2016) A possible restart of an interplate slow slip adjacent to the Tokai seismic gap in Japan. Earth Planets Space 68(54):00. https://doi.org/10.1186/s40623-016-0430-4
Sakaue H, Nishimura T, Fukuda J, Kato T (2019) Spatiotemporal evolution of long- and short-term slow slip events in the Tokai region, central Japan, estimated from a very dense GNSS network during 2013–2016. J Geophys Res Solid Earth 124(12):13207–13226. https://doi.org/10.1029/2019JB018650
Seshimo Y, Yoshioka S (2022) Spatiotemporal slip distributions associated with the 2018–2019 Bungo Channel long-term slow slip event inverted from GNSS data. Sci Rep 12:343. https://doi.org/10.1038/s41598-021-03982-6
Suenaga N, Yoshioka S, Matsumoto T (2016) Relationships among temperature, dehydration of the subducting Philippine Sea plate, and the occurrence of a megathrust earthquake, low-frequency earthquakes, and a slow slip event in the Tokai district, central Japan. Phys Earth Planet Inter 260:44–52
Wessel P, Smith WHF (1998) New, improved version of the generic mapping tools released. EOS Trans AGU 79:579
Yabuki T, Matsuura M (1992) Geodetic data inversion using a Bayesian information criterion for spatial distribution of fault slip. Geophys J Int 109:363–375
Yoshioka S, Mikumo T, Kostoglodov V, Larson KM, Lowryd AR, Singh SK (2004) Interplate coupling and a recent aseismic slow slip event in the Guerrero seismic gap of the Mexican subduction zone, as deduced from GPS data inversion using a Bayesian information criterion. Phys Earth Planet Inter 146:513–530
Yoshioka S, Matsuoka Y, Ide S (2015) Spatiotemporal slip distributions of three long-term slow slip events beneath the Bungo Channel, southwest Japan, inferred from inversion analyses of GPS data. Geophys J Int 201:1437–1455

Publisher's Note